J. Appl. Comput. Mech., 6(4) (2020) 1058-1068
DOI: 10.22055/JACM.2019.30677.1766

ISSN: 2383-4536
jacm.scu.ac.ir

M&MoCS

Shahid Chamran University of Ahvaz

Journal of Applied and Computational Mechanics

Research Paper

Spectral Quasi-linearization for MHD Nanofluid Stagnation Boundary Layer Flow due to a Stretching/Shrinking Surface

Hiranmoy Mondal[1], **Shipra Bharti**[2]

[1] Department of Mathematics, Brainware University, 398 Ramkrishnapur Road, Barasat, North 24 Parganas, Kolkata, West Bengal 700125, India, Email: hiranmoymondal@yahoo.co.in

[2] Durgapur Institute of Advanced Technology and Management, Maulana Abul Kalam Azad University of Technology B.Tech 3rd year, Department of Chemical Engineering, West Bengal 713212, India, Email: shiprabharti341999@gmail.com

Received August 14 2019 ; Revised November 15 2019 ; Accepted for publication November 15 2019.
Corresponding author: H. Mondal (hiranmoymondal@yahoo.co.in)

Abstract. This article concentrates on the effect of MHD heat mass transfer on the stagnation point nanofluid flow over a stretching or shrinking sheet with homogeneous-heterogeneous reactions. The flow analysis is disclosed in the neighborhood of stagnation point. Features of heat transport are characterized with Newtonian heating. The homogeneous-heterogeneous chemical reaction between the fluid and diffusing species is included in the mass diffusion equation. The MHD stagnation boundary layer flow is explored in the presence of heat generation/absorption. Numerical convergent solutions are computed via the spectral quasi-linearization method (SQLM). The physical aspects of different parameters are discussed through graphs.

Keywords: Melting heat transfer; Chemical reaction; Nanofluids; Stagnation point flow; Spectral quasilinearization method.

1. Introduction

The study of mixed convective flow heat and mass transfer through nanofluid stagnation point flow has important applications in industry and environmental sciences. The MHD stagnation nanofluid flow with homogeneous-heterogeneous chemical reaction has an application in engineering and sciences like petroleum industries, production of polymer and ceramics, fibrous insulation and agricultural lands. In view of these applications studies by Song [1] and Ikeda [2]. Williams et al. [3] and Kameswaran et al. [4] have established the model of homogeneous-heterogeneous chemical reaction with the effect of electric field. Hayat et al. [5] investigated the MHD ree-Eyring fluid in the co-ordinate system. The vast applications of magnetohydrodynamics (MHD) in the field of science, physical engineering processes, medicine, hydro pumps, separation of magnetic cells, optical gratings and MHD generators compels one to study its effect in the boundary layers flow problems. The strength and alignment of the magnetic field change the behavior of the boundary layer flow. The MHD nanofluid stagnation boundary layer flow has an important role in the recent trend of research areas. The significance in many areas such as the melting of permafrost, magma solidification, the heat exchanger coils around freezing of soil of a ground-based pump. Rahman et al. [6] described the features of the melting phenomenon in thermal radiation with MHD flow. Mostafa and Mahmoud [7] exposed the variation in stagnation nanofluid flow along a vertical stretching sheet. The impacts of different governing parameters on mixed convection flow of MHD activation energy thermal extrusion past stretching surfaces have been studied in [8] – [11].

The inviscid or viscous stagnation point exists in flows, regardless of being 2-D or 3-D, normal or oblique, forward or reverse, homogeneous or two immiscible fluid. The flow over the tips of rockets, aircraft, submarines, and oil ships, are the examples of stagnation point flow. Mukhopadhyay [12] analyzed the radiative effect with variable viscosity in

Published online: January 20 2020

stagnation point flow past a permeable stretching sheet. Whereas, there are very useful studies (see [13-24]) dealing with heat generation (or) absorption and stagnation point flow model together.

The homogeneous-heterogeneous chemical reactions depend on the reaction occurs in the bulk of the fluid (homogeneous) or on some catalytic surfaces (heterogeneous). The formation of homogeneous-heterogeneous chemical reactions are associated with the formation of reactant species at different rates both within the fluid and on the catalytic surfaces are complex. Das et al. [25] studied the Casson fluid with nonlinear stretching surfaces in the presence of homogeneous and heterogeneous reactions. Sithole et al. [26] studied heat and mass transfer with homogeneous-heterogeneous chemical reaction in the presence of nonlinear thermal radiation over a stretching sheet.

Literature surveys reveal that the MHD flow of a nanofluid in the stagnation point region with homogeneous-heterogeneous reaction is characterized via Newtonian heating. The mass transfer process is involved in the first-order chemical reaction. Variable fluid properties are implemented to study the heat and mass transport processes. The numerical solutions are explained in this paper through the spectral quasi-linearization method (see [27],[28]). The velocity, temperature and homogenous-heterogeneous species concentration profiles are demonstrated graphically and analyzed through different physical parameters.

2. Formulation

A model of 2-D magneto-nanofluid stagnation point flow over a stretching/shrinking sheet with the effect of homogeneous-heterogeneous chemical reactions was developed (see in Fig. 1). The stretching or shrinking sheet generates the flow due to the simultaneous application of two equal forces along the x-axis when the origin is fixed. The outside boundary layer velocity is $U_e = ax$, where $a > 0$ is the strength of the stagnation-point flow. The magnetic field of strength B_0 is externally applied normal to the sheet. The interaction of homogeneous and heterogeneous reactions involving two chemical species A and B in the boundary layer flow. In the forward stagnation point, the homogeneous reaction for cubic autocatalysis can be expressed as:

$$A + B \rightarrow 3A, \text{ rate } = k_1 C_a C_b^2,$$

while first-order isothermal reaction on the catalyst surface is presented in the following form:

$$A \rightarrow B, \quad \text{rate} = k_s C_a,$$

Here C_a and C_b are concentrations of chemical species A and B, k_1 is the homogeneous chemical reaction and k_s is the heterogeneous reaction rate. The external flow reactant A in which has a uniform concentration C_∞ .

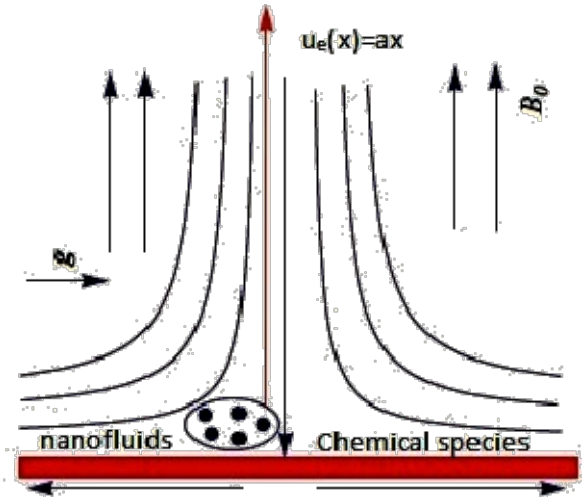

Fig. 1. The physical model and coordinate system

The chemical reaction of the outer edge in the boundary layer is assumed to be zero. Based on those assumptions, the equations for boundary layer MHD stagnation point flow for a nanofluid are written as:

$$\frac{\partial u}{\partial x} + \frac{\partial v}{\partial y} = 0, \tag{1}$$

$$u\frac{\partial u}{\partial x} + v\frac{\partial u}{\partial y} = U_e \frac{dU_e}{dx} + \nu\left(\frac{\partial^2 u}{\partial x^2} + \frac{\partial^2 u}{\partial y^2}\right) - \frac{\sigma B_0^{\,2}}{\rho}(u - u_e) \tag{2}$$

$$u\frac{\partial T}{\partial x}+v\frac{\partial T}{\partial y}=\alpha\left(\frac{\partial^2 T}{\partial x^2}+\frac{\partial^2 T}{\partial y^2}\right)+\tau D_B\left(\frac{\partial C_b}{\partial x}.\frac{\partial T}{\partial x}+\frac{\partial C_b}{\partial y}.\frac{\partial T}{\partial y}\right)+\tau\frac{D_T}{T_\infty}\left[\left(\frac{\partial T}{\partial x}\right)^2+\left(\frac{\partial T}{\partial y}\right)^2\right]+\frac{Q_0}{\sigma C_p}(T-T_\infty) \tag{3}$$

$$u\frac{\partial C_a}{\partial x}+v\frac{\partial C_b}{\partial y}=D_A\left(\frac{\partial^2 C_a}{\partial x^2}+\frac{\partial^2 C_a}{\partial y^2}\right)-k_1 C_a C_b^{\,2} \tag{4}$$

$$u\frac{\partial C_b}{\partial x}+v\frac{\partial C_b}{\partial y}=D_B\left(\frac{\partial^2 C_b}{\partial x^2}+\frac{\partial^2 C_b}{\partial y^2}\right)+\frac{D_T}{T_\infty}\left(\frac{\partial^2 T}{\partial x^2}+\frac{\partial^2 T}{\partial y^2}\right)+k_1 C_a C_b^{\,2} \tag{5}$$

where u and v are the velocity, ν is the kinematic viscosity, σ is the electric conductivity, τ is the ratio of the effective heat capacity of nanoparticle to that of the fluid, ρ is the fluid density, T and T_w are the fluid and melting surface temperatures, T_∞ is temperature at the outer edge of the boundary layer and D_T is the thermophoresis diffusion coefficient. The corresponding boundary conditions are:

$$\begin{gathered}u=U_W(x),\ v=v_W,\ T=T_\infty,\ D_A\frac{\partial C_a}{\partial y}=k_s C_a,\ D_B\frac{\partial C_b}{\partial y}=-k_s C_a \ at\ y=0\\ u\to U_e=ax(a>0),T\to T_\infty,C_a\to C_\infty,C_b\to 0,\ as\ y\to\infty\end{gathered} \tag{6}$$

Using the following non-dimensional variables:

$$u=axf'(\eta),\ v=-(av)^{1/2}f(\eta),\ \ \theta(\eta)=\frac{T-T_\infty}{T_W-T_\infty},\ \ \xi(\eta)=\frac{C_a}{C_\infty},\ \ \varphi(\eta)=\frac{C_b}{C_\infty},\ \ \eta=\left(\frac{a}{\nu}\right)^{1/2}y, \tag{7}$$

where f, θ, ξ and φ are the dimensionless velocity, temperature, concentration of chemical species A and B respectively. Using Eqs. (10), the continuity Eq. (3) is identically satisfied and Eqs. (4) to (7) reduce to:

$$f'''+f''f+1-f'^2+Ha^2(1-f')=0 \tag{8}$$

$$\frac{1}{\mathrm{Pr}}\theta''+N_b\theta'\varphi'+N_t\theta'^2+f\theta'+\delta\theta=0 \tag{9}$$

$$\frac{1}{Sc}\xi''+f\xi'-K\xi\varphi^2=0 \tag{10}$$

$$\frac{1}{\varepsilon Sc}\left(\varphi''+\frac{Nt}{Nb}\theta''\right)+f\varphi'+K\xi\varphi^2=0 \tag{11}$$

where $Ha=B_0\sqrt{\sigma/(\rho a)}$ is the Hartmann number, $\mathrm{Pr}=\upsilon/\alpha$ is the Prandtl number, $Nb=\tau D_B C_\infty/\upsilon$ is the Brownian motion parameter, $Nt=\tau D_T(T_w-T_\infty)/\upsilon T_\infty$ is the thermophoresis parameter, $\delta=Q_0/a\rho C_p$ is the heat generation/absorption parameter, $Sc=\upsilon/D_A$ is the Schimdt number, $K=k_1C_\infty^2/a$ is the homogeneous reaction rate parameter, $K_s=k_s/D_B(a/\nu)^{-1/2}$ is the heterogeneous reaction rate parameter, $\varepsilon=D_A/D_B$ is the ratio of the diffusion coefficient, $\lambda=m/a$ is the stretching rate of external flow rate where $\lambda>0$ corresponds to a stretching surface and $\lambda<0$ corresponds to a shrinking surface and $S=-v_w/(av)^{1/2}$ is the mass transfer parameter with $S>0$ for suction, $S<0$ for injection and $S=0$ for an impermeable surface. The boundary conditions of the problem are as follows:

$$\begin{gathered}f(0)=S,\ f'(0)=\lambda,\ \ \theta(0)=1,\ \ \xi'(0)=K_S\xi(0),\ \ \ \varphi'(0)=-\varepsilon K_S\xi(0)\\ f'(\infty)=1,\ \theta(\infty)=0,\ \ \xi(\infty)=1,\ \ \varphi(\infty)=0\end{gathered} \tag{12}$$

The physical quantity of interest here is the skin friction coefficient C_f and Nusselt number Nu_x which are defined as:

$$C_f=\frac{\tau_W}{\rho U_e^{\,2}},\ \ \tau_W=\mu\left(\frac{\partial u}{\partial y}\right)_{y=0},\ \ \mathrm{Re}_x^{1/2}C_f=f''(0) \tag{13}$$

$$Nu_x = \frac{xq_W}{k(T_W - T_\infty)},\ q_W = -k\left(\frac{\partial T}{\partial y}\right)_{y=0},\ \mathrm{Re}_x^{-1/2} Nu_x = -\theta'(0) \tag{14}$$

where τ_w and q_w are the stress of shear at the surface and heat transfer from the sheet, $\mathrm{Re}_x = xU_e/\nu$ is the Reynolds number.

3. Numerical Solution using Spectral Quasi-linearization Method (SQLM)

The coupled system of equations (10)-(13) were solved using the spectral quasi-linearization method. The nonlinear components of the Eqs. (10)-(13) give the following iterative sequence of linear differential equations:

$$a_{0,r} f'''_{r+1} + a_{1,r} f''_{r+1} a_{2,r} f'_{r+1} + a_{3,r} f_{r+1} = R_f \tag{15}$$

$$b_{0,r}\theta''_{r+1} + b_{1,r}\theta'_{r+1} + b_{2,r}\theta_{r+1} + b_{3,r} f_{r+1} + b_{4,r}\xi_{r+1} = R_\theta \tag{16}$$

$$c_{0,r}\xi''_{r+1} + c_{1,r}\xi'_{r+1} + c_{2,r}\xi_{r+1} + c_{3,r} f_{r+1} + c_{4,r}\varphi_{r+1} = R_\xi \tag{17}$$

$$d_{0,r}\varphi''_{r+1} + d_{1,r}\varphi'_{r+2} + d_{2,r}\varphi_{r+1} + d_{3,r} f_{r+1} + d_{4,r}\theta''_{r+1} = R_\varphi \tag{18}$$

where the coefficients $a_{s1,r}(s1 = 0,1,2,3)$, $b_{s1,r}(s1 = 0,1,2,3)$, $c_{s1,r}(s1 = 0,1,2,3)$ and $d_{s1,r}(s1 = 0,1,2,3)$ are known functions and are defined as:

$$a_{0,r} = 1,\ a_{1,r} = f_r,\ a_{2,r} = -2f' - Ha^2,\ a_{3,r} = f_r'',$$

$$b_{0,r} = 1, b_{1,r} = \mathrm{Pr}\, f_r + 2P_r N_t \theta_r' - P_r Nb\xi_r',\ b_{2,r} = \mathrm{Pr}\,\delta,\ b_{3,r} = \mathrm{Pr}\,\theta_r',\ b_{4,r} = -\mathrm{Pr}\, Nb\theta_r'$$

$$c_{0,r} = 1,\ c_{1,r} = Scf_r,\ c_{2,r} = -ScK\varphi_r^2,\ c_{3,r} = Sc\xi_r',\ c_{4,r} = Sc\xi',$$

$$d_{0,r} = 1,\ d_{1,r} = \varepsilon Scf_r,\ d_{2,r} = 2\varepsilon ScK\xi_r\varphi_r,\ d_{3,r} = \varepsilon Sc\varphi_r',\ d_{4,r} = Nt/Nb$$

$$R_f = a_{0,r} f''' + a_{1,r} f_r'' + a_{2,r} f_r' + a_{3,r} f_r - F,$$

$$R_\theta = b_{0,r}\theta_r'' + b_{1,r}\theta_r' + b_{2,r}\theta_r + b_{3,r} f_r'' + b_{4,r} f_r' + b_{5,r}\xi_r' - \Theta,$$

$$R_\xi = c_{0,r}\xi_r'' + c_{1,r}\xi_r'' + c_{2,r}\xi_r + c_{3,r} f_r + c_{4,r}\varphi_r - \chi$$

$$R_\varphi = d_{0,r}\varphi_r'' + d_{1,r}\varphi_r'' + d_{2,r}\varphi_r + d_{3,r} f_r + d_{4,r}\theta_r'' - \psi$$

subject to the boundary conditions:

$$\begin{gathered} f_{r+1}(0) = S,\ f'_{r+1}(0) = \lambda,\ \theta_{r+1}(0) = 1,\ \ \xi'_{r+1}(0) = K_s\xi_{r+1}(0),\ \ \varphi'_{r+1}(0) = -\varepsilon K_s\xi(0), \\ f'_{r+1}(\infty) = 1,\quad \theta_{r+1}(\infty) = 0,\quad \xi_{r+1}(\infty) = 1,\ \ \varphi_{r+1}(\infty) = 0, \end{gathered} \tag{19}$$

The system of equations (17) to (20) are chosen as functions that satisfy the boundary conditions as follows:

$$f_0 = \eta + S + (1-\lambda)\left(e^{-\eta} - 1\right),\ \theta_0 = e^{-\eta},\ \ \xi_0 = 1 - \frac{K_s}{1+K_s}e^{-\eta},\ \ \varphi_0 = \varepsilon\frac{K_s}{1+K_s}e^{-\eta} \tag{20}$$

Similarly, the vectors Θ_i, χ_i and ψ_i are defined as:

$$\Theta_i = \left[\theta(\eta_0), \theta(\eta_1), \ldots, \theta\left(\eta_{N_x}\right)\right]^t \tag{21}$$

$$\chi_i = \left[\chi(\eta_0), \chi(\eta_1), \ldots, \chi\left(\eta_{N_x}\right)\right]^t \tag{22}$$

$$\psi_i = \left[\varphi(\eta_0), \varphi(\eta_1), ..., \varphi\left(\eta_{N_z}\right)\right]^t \tag{23}$$

The superscript t in equation denotes the transpose matrix. Applying the quasi-linearization technique gives the following system of equations:

$$A_{11}F + A_{12}\Theta + A_{13}\chi + A_{14}\psi = R_f \tag{24}$$

$$A_{21}F + A_{22}\Theta + A_{23}\chi + A_{24}\psi = R_\theta \tag{25}$$

$$A_{31}F + A_{32}\Theta + A_{33}\chi + A_{34}\psi = R_\chi, \tag{26}$$

$$A_{41}F + A_{42}\Theta + A_{43}\chi + A_{44}\psi = R_\varphi, \tag{27}$$

Applying the spectral method as described above gives a matrix of size $\left(N_x+1\right)\times\left(N_x+1\right)$ with:

$$\begin{bmatrix} A_{11} & A_{12} & A_{13} & A_{14} \\ A_{21} & A_{22} & A_{23} & A_{24} \\ A_{31} & A_{32} & A_{33} & A_{34} \\ A_{41} & A_{42} & A_{43} & A_{44} \end{bmatrix} \begin{bmatrix} f_{r+1} \\ \theta_{r+1} \\ \xi_{r+1} \\ \varphi_{r+1} \end{bmatrix} = \begin{bmatrix} R_f \\ R_\theta \\ R_\xi \\ R\varphi \end{bmatrix} \tag{28}$$

The approximate solutions for F, Θ, χ and ψ are obtained by solving the above system of equations after applying appropriate boundary conditions.

4. Results and Discussion

The system of nonlinear differential Eqs. (11) to (14) together with boundary conditions (15) and (16) solved by using the spectral quasi-linearization method (SQLM) for different parameter values. Results for a stretching sheet are compared with Wang [24], Ishak et al. [25] and Shaw et al. [26] in Table 1, and for the shrinking sheet with Rosali et al. [27] and Bhattacharyya [10] in Table 2. There is an excellent agreement with the present results. The results show that the existence and uniqueness of the non-linear solution depend on the stretching/shrinking parameter. It is clear from Table 1 that the positive values of the skin friction coefficient decrease for $\lambda<1$, and are negative when $\lambda>1$. Physically, the negative values of $f''(0)$ correspond to the surface exerting a drag force on the fluid and the positive sign implies the opposite. The skin friction coefficient $f''(0)$ is zero when $\lambda=1$ meaning the cylinder and fluid move with the same velocity. From Table 2, the skin friction coefficient $f''(0)$ increases for some values of λ, but decreases after a certain value of λ.

Table 1. Comparison of $f''(0)$ for different values of the stretching parameter.

λ	Wang [29]	Ishak [30]	Shaw et al. [31]	Present Results
0	1.23258	1.232588	1.23258766	1.23259
0.5	0.71330	0.713295	0.71329496	0.71329
2	-1.88731	-1.887307	-1.8873066	-1.88730
5	-10.26475	-10.264749	-10.264749	-10.2650

Table 2. Comparison of $f''(0)$ for different values of the shrinking parameter.

λ	Rosali et al. [32]	Shaw et al. [31]	Bhattacharyya [33]	Present Results
-0.25	1.402241	1.40224081	1.4022405	1.4022
-0.75	1.489298	1.48929824	1.4892981	1.4893
-1.05	1.266228	1.26622794	---	1.2662
-1.15	1.082231	1.08223117	1.0822316	1.0822

Figures 2-4 show the effect of iterations on residual errors of f, θ, ξ and φ. It is observed that as the number of iterations increase, the errors reduce significantly using the method of spectral quasi-linearization. The accuracies of the SQLM can be determined by calculating the residual error of the methods. The residual error is used to determine how close the approximate solution is to the true solution of the differential equation. We considered the maximum residual error hence the choice of the infinity norm when calculating the residual error. These figures show the residual error of the SQLM for different values of suction or suction/injection parameter S. It can be seen that within this time interval, the method maintains a very high accuracy as they have a residual error of 10^{-10}.

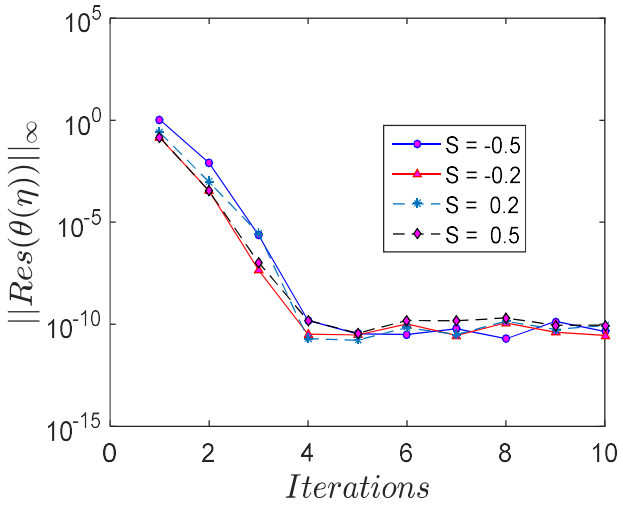

Fig. 2. Effects of S on residual error $\theta(\eta)$.

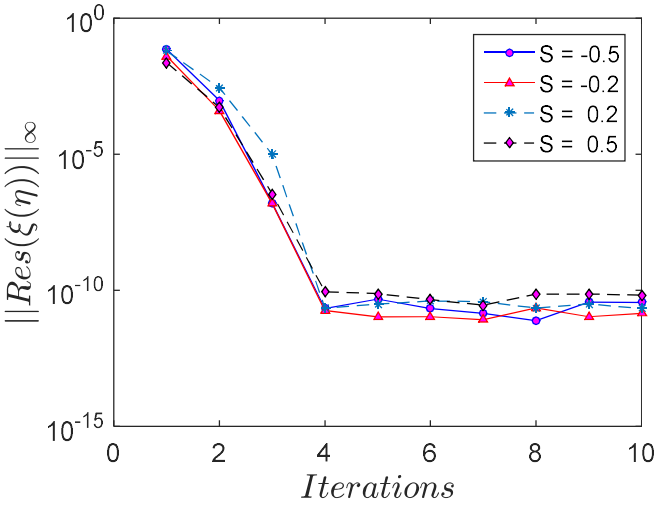

Fig. 3. Effects of S on residual error $\xi(\eta)$.

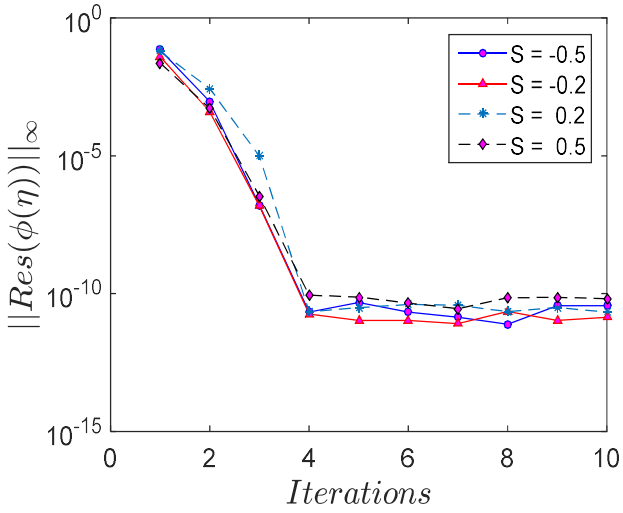

Fig. 4. Effects of S on residual error $\varphi(\eta)$.

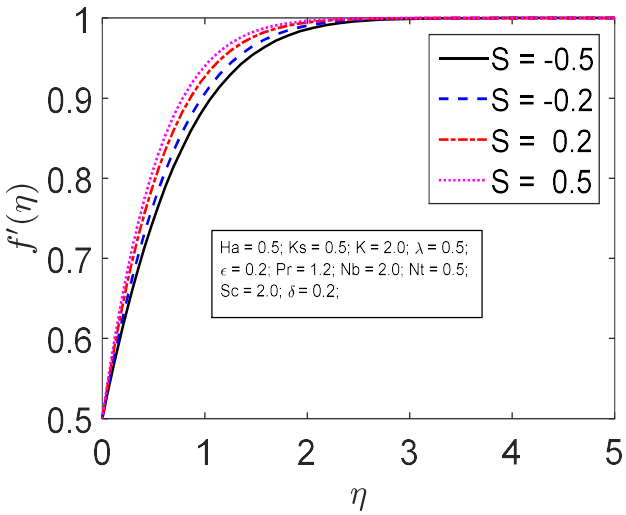

Fig. 5. Velocity profiles for various values of the suction parameter S.

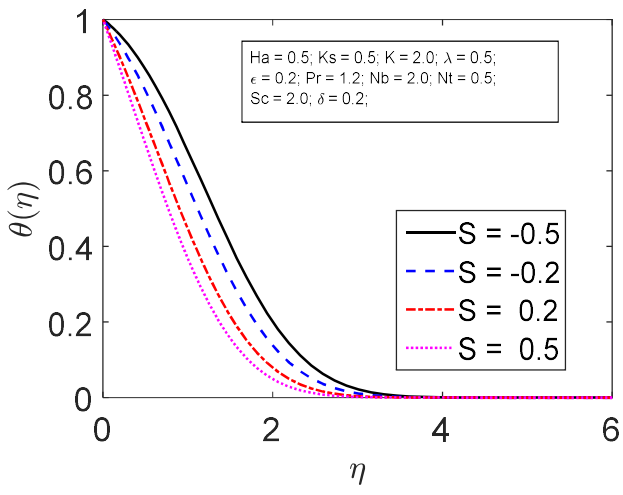

Fig. 6. Temperature profiles for various values of the suction parameter S.

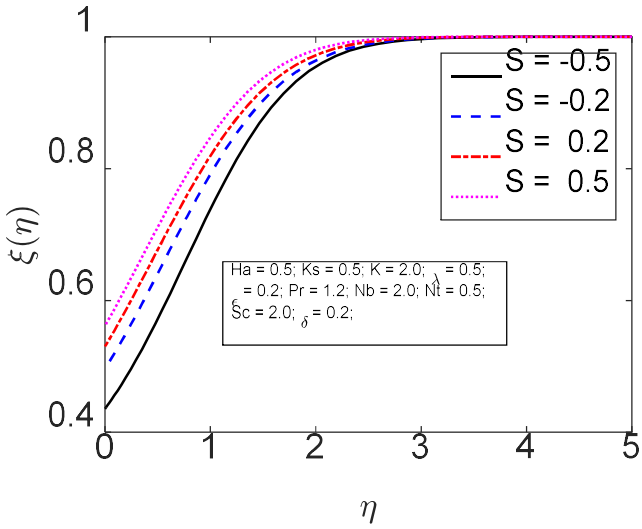

Fig. 7. The concentration of chemical species A for various values of the suction parameter S.

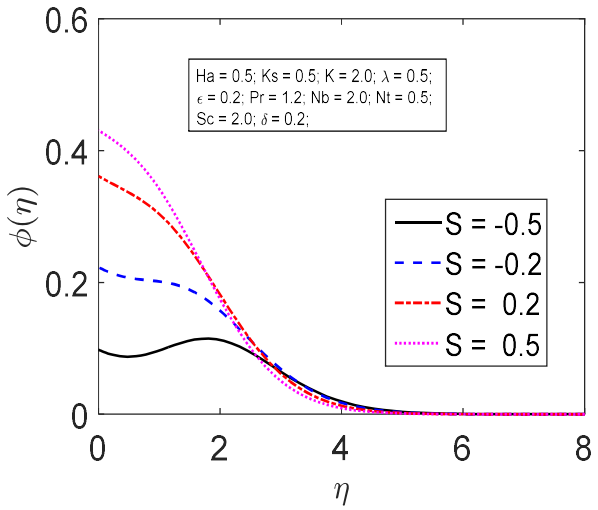

Fig. 8. The concentration of chemical species B for various values of the suction parameter S.

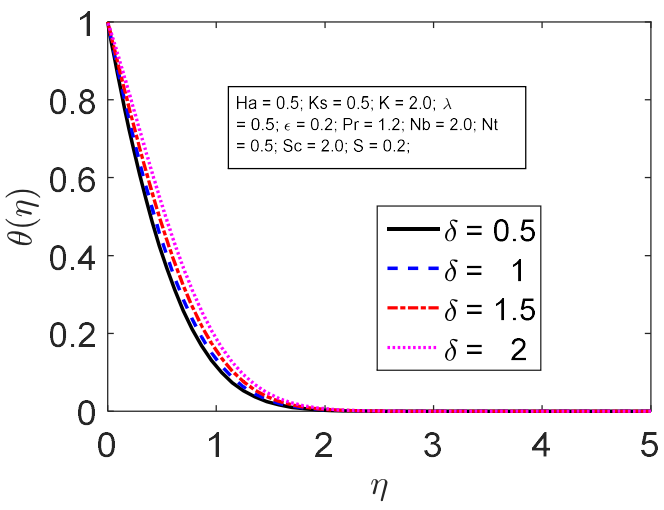

Fig. 9. Temperature profiles for various values of the heat generation parameter δ.

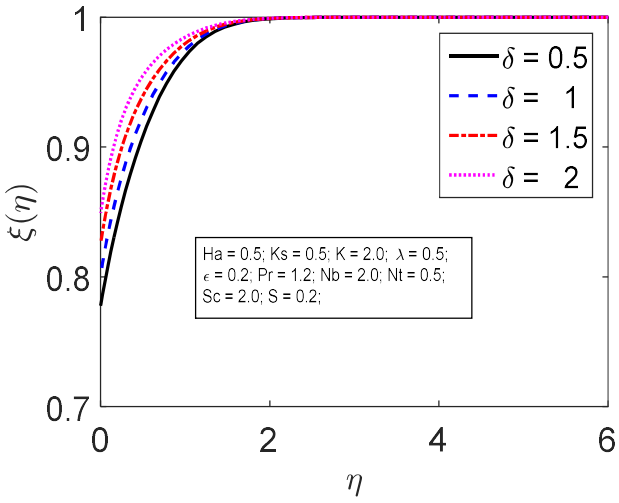

Fig. 10. The concentration of chemical species A for various values of the heat generation parameter δ.

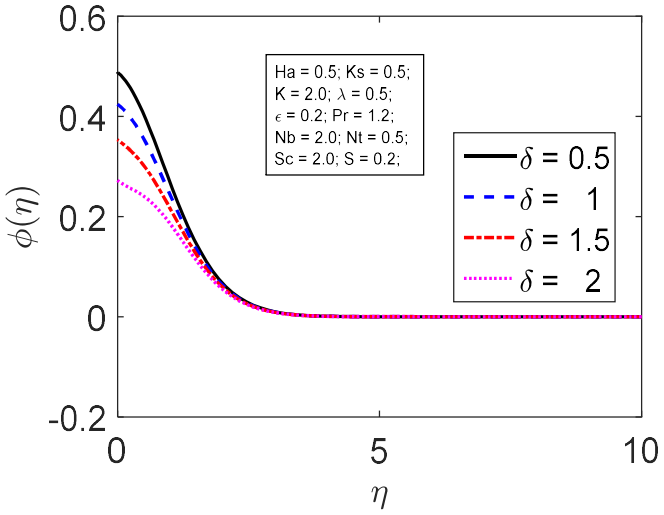

Fig. 11. The concentration of chemical species B for various values of heat generation parameter δ.

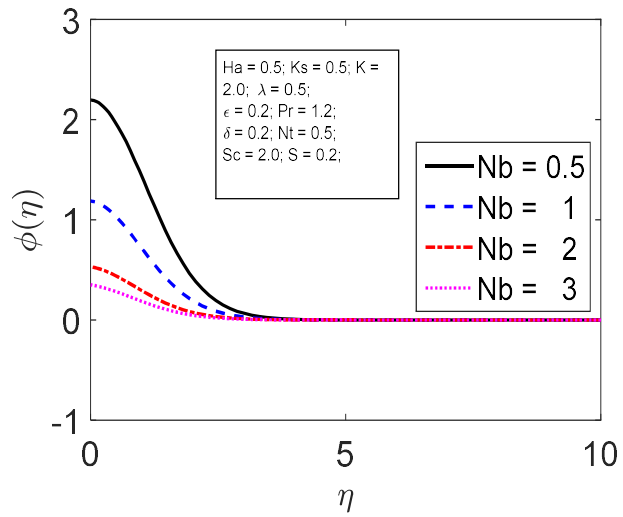

Fig. 12. The concentration of chemical species B for various values of Brownian motion parameter Nb.

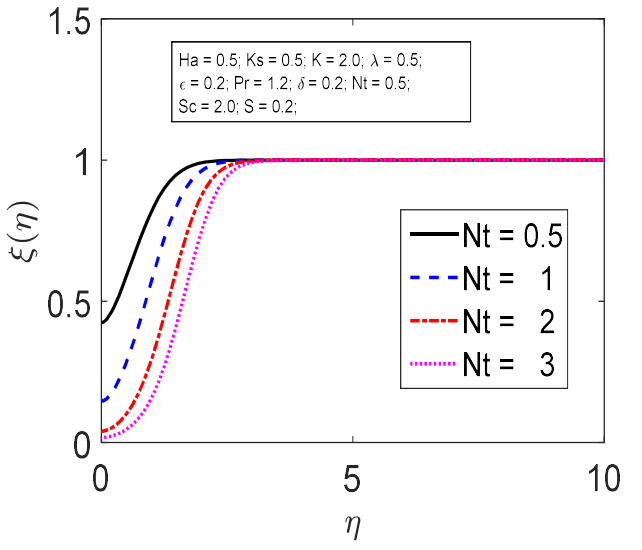

Fig. 13. The concentration of chemical species A for various values of thermophoresis parameter Nt.

The impact of the suction parameter S on the velocity, temperature and concentration profiles is shown in Figures 5-8. It is analyzed that with an increase in S, the velocity and concentration profiles of chemical species A increase due to the decrease of kinematic viscosity whereas the opposite behavior is noted for the temperature profiles. The concentration of chemical species B increase when the similarity transformation $\eta \geq 2$. The concentration boundary layer thickness decreases as the suction parameter increases.

The effects of the melting heat generation/absorption parameter on temperature and concentration profiles are presented in Figures 9-11. The higher values of the melting parameter lead to an enhancement of the thermal boundary layer thickness of $\theta(\eta)$ and concentration species A. The chemical species B and the concentration profiles decrease with an increase in melting heat generation/absorption parameter δ.

Figure 12 shows the effect of Brownian motion parameter Nb on the concentration of chemical species B. The effect of increasing Nb is to decrease the concentration of chemical species B due to diffusion of chemical species of the heterogeneous chemical reaction. Figure 13 illustrates that the concentration profiles $\xi(\eta)$ for different values thermophoresis parameter Nt. The chemical species A decreases with increasing the thermophoresis parameter due to a decrease in the free stream temperature.

The influence of homogeneous reaction rate parameter K on the concentration of chemical species A and B are sketched in Figure 14-15. The concentration profile of decreases while boundary layer thickness increases for higher values of K whereas the reverse effect is seen in Figure 15 for chemical species B. The impact of the strength of the heterogeneous reaction parameter Ks on the concentration distribution is shown in Figure 16-17. The chemical species A decreases near the surface of the cylinder and increases away from the surface for higher values of the heterogeneous reaction parameter Ks.

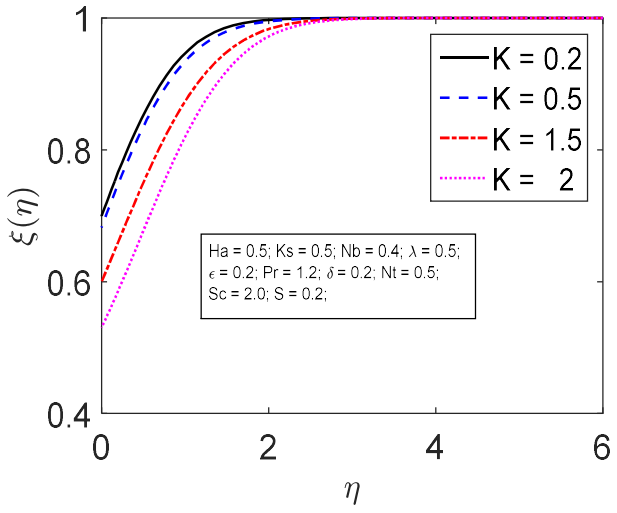

Fig. 14. The concentration of chemical species A for various values of homogeneous reaction rate parameter K.

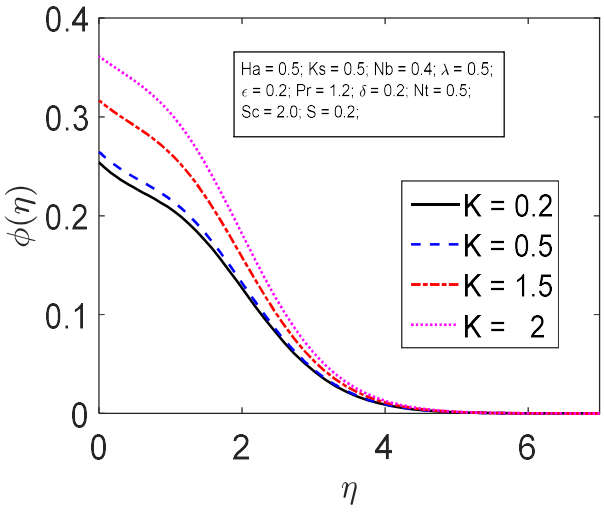

Fig. 15. The concentration of chemical species B for various values of homogeneous reaction rate parameter K.

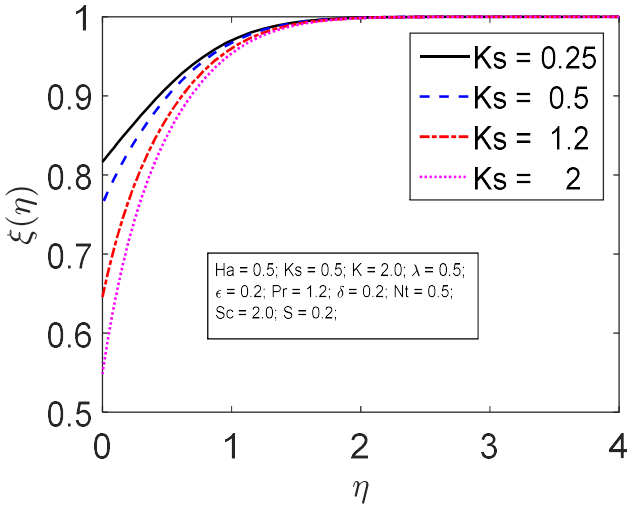

Fig. 16. The concentration of chemical species A for various values of heterogeneous reaction rate parameter Ks.

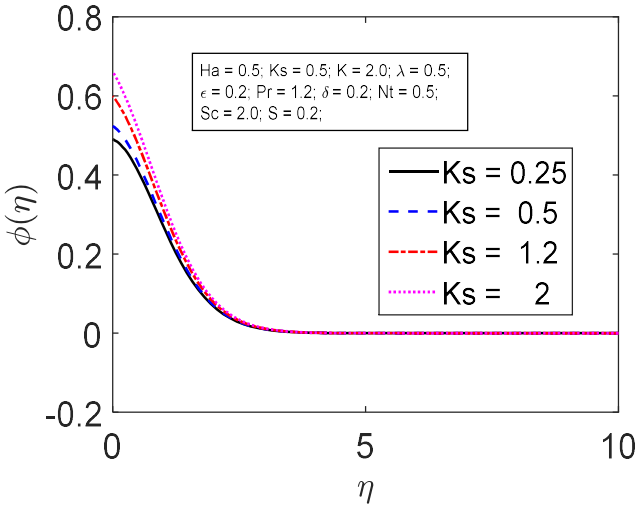

Fig. 17. The concentration of chemical species B for various values of heterogeneous reaction rate parameter Ks.

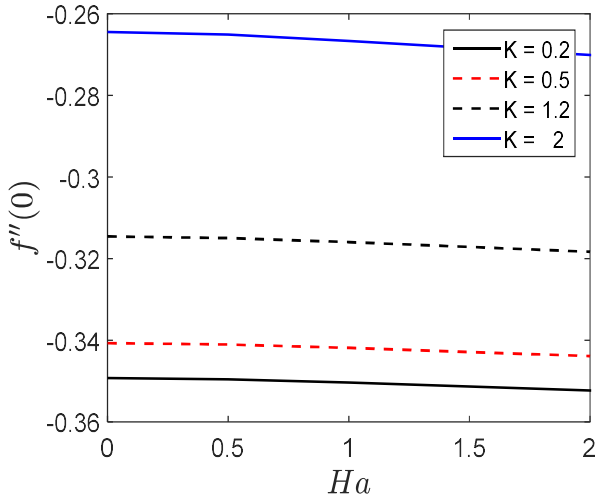

Fig. 18. Skin-friction coefficient against *Ha* for different values of *K*.

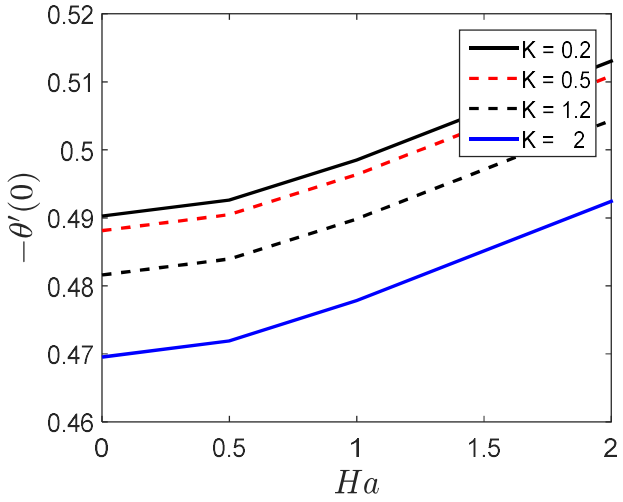

Fig. 19. Nusselt number against *Ha* for different values of *K*.

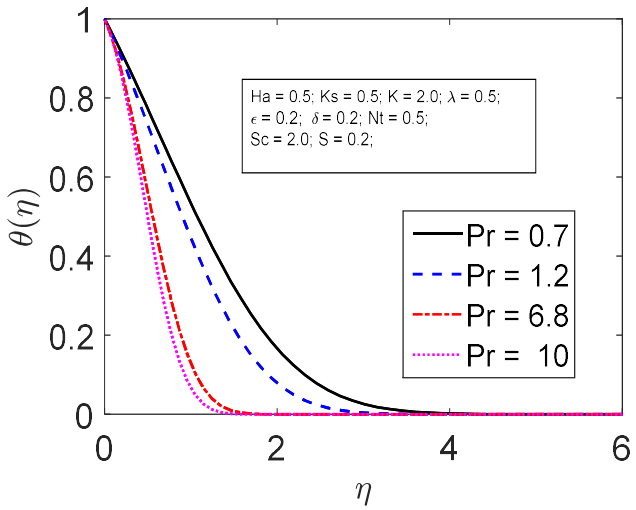

Fig. 20. Variation of temperature profile for different values of Prandtl number Pr.

Figure 18 presents the variation of the skin friction coefficient with homogeneous chemical reaction *K* for different values of *Ha (*Hartmann number*)*. From this figure, it is evident that the absolute values of the skin friction coefficient increase as *K* increased. But the reverse effect is seen in Figure 19 that the variation of the gradient of temperature at the surface $-\theta'(0)$ decrease with the increase the homogeneous chemical reaction *K* for different values of Hartmann number *Ha*. Figure 20 represents the graph of the Prandtl number on temperature profiles. The temperature profile decreases due to the decrease of the thermal diffusivity. The increment of Pr means the slow down of the rate of thermal diffusion.

5. Concluding Remarks

The characteristics of homogeneous-heterogeneous chemical reactions with heat generation in stagnation boundary-layer nanofluid flow was investigated. The dimensionless nonlinear differential equations were solved numerically using the SQLM method. Flow was two dimensional MHD over a stretching surface. The following observations are worth mentioning:

(i) Velocity profiles and concentration of chemical species are enhanced when the suction parameter increases.

(ii) Temperature distribution increases for higher values of the melting parameter.

(iii) As the value of the homogeneous reaction rate parameter increases, the concentration of the chemical species decreases.

(iv) Higher values of the heterogeneous reaction rate parameter result in the enhancement of concentration profiles.

Author Contributions

H. Mondal planned the scheme and developed the mathematical model. S. Bharti examined the theory validation. The manuscript was written through the contribution of all authors. All authors discussed the results, reviewed and approved the final version of the manuscript.

Acknowledgments

The authors wish to express their thanks to the competent anonymous of the editors and referees for their valuable comments and suggestions. The authors also acknowledge the Department of Mathematics to encourage the research in Brainware University, Barasat, Kolkata.

Conflict of Interest

The authors declared no potential conflicts of interest with respect to the research, authorship, and publication of this article.

Funding

The authors received no financial support for the research, authorship, and publication of this article.

References

[1] Song, X., Williams,W. R., Schmidt, L. D., Aris, R., Bifurcation behavior in homogeneous-heterogeneous combustion: II. Computations for stagnation-point flow, *Combustion Flame*, 84(3-4), 1991, 292-311.
[2] Ikeda, H., Libby, P.A., Williams, F.A., Catalytic combustion of hydrogen-air mixtures in stagnation flows. *Combustion Flame*, 93, 1993, 138-148,.
[3] Williams,W.R., Stenzel,M.T., Song, X., Schmidt, L.D., Bifurcation behavior in homogeneous-heterogeneous combustion. I. Experimental results over platinum, *Combustion Flame*, 84, 1991, 277-291.
[4] Kameswaran,P.K., Shaw,S., Sibanda, P., Murthy, P.V.S.N., Homogeneous-heterogeneous reactions in a nanofluid flow due to a porous stretching sheet, *Int J Heat Mass Transfer*, 57(2), 2013, 465-472.
[5] Hayat, T., Akram,J., Alsaedi, A., Zahir, H., Endoscopy and homogeneousheterogeneous reactions inMHD radiative peristaltic activity of Ree-Eyring fluid, *Results in Physics*, 8**,** 2018, 481-488.
[6] Rahman,R. G. A. Khadar, M. M., Megahed, A. M., Melting phenomenon in magnetohydrodynamics steady flow and heat transfer over a moving surface in the presence of thermal radiation, *Chin Phys B*, 22, 2013, 030202.
[7] Mostafa, A., Mahmoud, A., Heat and mass transfer in stagnation-point flow towards a vertical stretching sheet embedded in a porous medium with variable fluid properties and surface slip velocity. *Chem Eng Commun*, 200, 2012, 543-62.
[8] Hsiao, K.L., To promote radiation electrical MHD activation energy thermal extrusion manufacturing system efficiency by using Carreau-Nanofluid with parameters control method*, Energy,* 130, 2017, 486-499.
[9] Hsiao, K.L., Combined Electrical MHD Heat Transfer Thermal Extrusion System Using Maxwell Fluid with Radiative and Viscous Dissipation Effects, *Applied Thermal Engineering*, doi: 10.1016/j.applthermaleng.2016.08.208.
[10] Hsiao, K.L., Micropolar nanofluid flow with MHD and viscous dissipation effects towards a stretching sheet with multimedia feature, *International Journal of Heat and Mass Transfer*, 112, 2017, 983-990.
[11] Hsiao, K.L., Stagnation electrical MHD nanofluid mixed convection with slip boundary on a stretching sheet, *Applied Thermal Engineering*, 98, 2016, 850-861.
[12] Mukhopadhyay, S., Effects of thermal radiation and variable fluid viscosity on stagnation point flow past a porous stretching sheet, *Meccanica*, 48, 2013, 1717-1730.
[13] Rostami,M., Dinarv, S., Pop, I., Dual solutions for mixed convective stagnation-point flow of an aqueous silica–alumina hybrid nanofluid. *Chinese Journal of Physics*, 56(5), 2018, 2465-2478.
[14] Akbar, N.S., Nadeem, S., UlHaq, R., Shiwei, Ye, MHD stagnation point flow of Carreau fluid toward a permeable shrinking sheet: Dual solutions, *Ain Shams Engineering Journal*, 5(4), 2014, 1233-1239.
[15] Elnajjar, E.J., Qasem, M. A., Fathi, M.A., Unsteady flow and heat transfer characteristics of fluid flow over a shrinking permeable infinite long cylinder, *Journal of Heat Transfer*, 138(9), 2016, 091008.
[16] Mondal, H., Almakki, M., Sibanda, P., Dual solution for three-dimensional MHD nanofluid flow with entropy generation, *Journal of Computational Design and Engineering*, doi: 10.1016/j.jcde.2019.01.003.
[17] Al Sakkaf, L.Y., Qasem, M.A., Al Khawaja, U.A., A Numerical Algorithm for Solving Higher-Order Nonlinear BVPs with an Application on Fluid Flow over a Shrinking Permeable Infinite Long Cylinder, *Complexity*, 2018, 2018, 1-11.
[18] RehmanI K,U., Shahzadi, M.Y., Qasem M.A., Mostafa, Z., On heat transfer in the presence of nano-sized particles suspended in a magnetized rotatory flow field, *Case Studies in Thermal Engineering*, 14, 2019, 100457.
[19]Rehman, K.U., Qasem, M. A., Malik, M. Y., Symmetry analysis on thermally magnetized fluid flow regime with heat source/sink, *Case Studies in Thermal Engineering*, 14, 2019, 100452.
[20] Vishnu, G. N., Qasem, M.A., SaraAl, F., Shymaa, D., Riga–Plate flow of γ Al2O3-water/ethylene glycol with effective Prandtl number impacts, *Heliyon*, 5(5), 2019, 01651.
[21] Ganesh, N. V., Qasem M. A., Ali J. C., A numerical investigation of Newtonian fluid flow with buoyancy, thermal slip of order two and entropy generation, *Case Studies in Thermal Engineering,* 13, 2019, 100376.

[22] Ganesh, N.V., Kameswaran, P. K., Al-Mdallal, Q.M., Hakeem, A. K. A., Ganga, B., Non-Linear thermal radiative marangoni boundary layer flow of gamma Al2O3 nanofluids past a stretching sheet, *Journal of Nanofluids*, 7(5), 2018, 944-950.
[23] Ganesh, N. V., Qasem M. A., Kameswaran, P. K., Numerical study of MHD effective Prandtl number boundary layer flow of Al_2O_3 nanofluids past a melting surface, *Case Studies in Thermal Engineering*, 13, 2019, 100413.
[24] Ganesh, N. V., Hakeem, A. A., Ganga. B., Darcy–Forchheimer flow of hydromagnetic nanofluid over a stretching/shrinking sheet in a thermally stratified porous medium with second order slip, viscous and Ohmic dissipations effects*, Ain Shams Engineering Journal*, 9(4), 2018, 939-951.
[25] Das, S., Mondal, H., Kundu, P.K., Sibanda, P., Spectral quasilinearization method for Casson fluid with homogeneous-heterogeneous reaction in presence of nonlinear thermal radiation over an exponential stretching sheet, *Multidiscipline Modeling in Materials and Structures*, 15(2), 2019, 398-417.
[26] Sithole, H., Mondal, H., Magagul, V.M., Sibanda, P., Motsa, S., Bivariate spectral local linearisation method (BSLLM) for unsteady MHD micropolar-nanofluids with homogeneous-heterogeneous chemical reactions over a stretching surface, *International Journal of Applied and Computational Mathematics*, 5, 2019, 5-12
[27] Mondal, H., Mishra, S., Kundu, P.K., Sibanda, P., Entropy generation of variable viscosity and thermal radiation on magneto nanofluid flow with dusty fluid, *Journal of Applied and Computational Mechanics*, 6(1), 2020, 171-182.
[28] Pal, D., Mondal, S., Mondal, H.**,** Entropy generation on MHD Jeffrey nanofluid over a stretching sheet with nonlinear thermal radiation using spectral quasilinearization Method, *International Journal of Ambient Energy*, 2019, doi: 10.1080/01430750.2019.1614984.
[29] Wang, C.Y., Stagnation flow towards a shrinking sheet, *Int J Non-Linear Mech*, 43, 2008, 377-382.
[30] Ishak, A., Lok, Y.Y., Pop, I., Stagnation point flow over a shrinking sheet in a micropolar fluid, *Chem En g Commun*, 197, 2010, 1417-1427.
[31] Shaw,S., Kameswaran, P. K., Sibanda, P., Homogeneous-heterogeneous reactions in micropolar fluid flow from a permeable stretching or shrinking sheet in a porous medium, *Boundary Value Problems*, 77, 2013, 1-10.
[32] Rosali, H., Ishak, A., Pop.I., Micropolar fluid flow towards a stretching/shrinking sheet in a porous medium with suction, *Int Commun Heat Mass Transf*, 39, 2012, 826-829.
[33] Bhattacharyya, K., Dual solutions in boundary layer stagnation-point flow and mass transfer with chemical reaction past a stretch-ing/shrinking sheet, *Int Communications in Heat and Mass Transfer*, 38, 2011, 917-922.

ORCID iD

Hiranmoy Mondal https://orcid.org/0000-0002-9153-300X
Shipra Bharti https://orcid.org/0000-0003-2641-6007

How to cite this article: Mondal, H., Bharti, S. Spectral Quasi-linearization for MHD Nanofluid Stagnation Boundary Layer Flow due to a Stretching/Shrinking Surface, *J. Appl. Comput. Mech.*, 6(4), 2020, x–xx.
https://doi.org/10.22055/JACM.2019.30677.1766